THE AMERICAN SOCIETY OF MECHANICAL ENGINEERS
345 E. 47th St., New York, N.Y. 10017

97-GT-319

CREEP LIFE PREDICTION OF CERAMIC COMPONENTS SUBJECTED TO TRANSIENT TENSILE AND COMPRESSIVE STRESS STATES

Osama M. Jadaan
University of Wisconsin-Platteville
Platteville, WI 53818

Lynn M. Powers
Case Western Reserve University
Cleveland, OH 44106

John P. Gyekenyesi
NASA Lewis Research Center
Cleveland, OH 44135

ABSTRACT

The desirable properties of ceramics at high temperatures have generated interest in their use for structural applications such as in advanced turbine systems. Some of these ceramic components, such as vanes and rotors, are subjected to concurrent tensile and compressive stress fields. Design lives for such systems can exceed 10,000 hours. Such long life requirements necessitate subjecting the components to relatively low stresses. The combination of high temperatures and low stresses typically places failure for monolithic ceramics in the creep regime. The objective of this paper is to present a design methodology for predicting the lifetimes of structural components subjected to concurrent transient tensile and compressive creep stress states. In this methodology, failure generally starts at or near the most highly stressed point and subsequently propagates across the section. The creep rupture life is divided into two stages. The first is called the stage of latent failure. During this stage the damage accumulates until it becomes critical at some point within the component, and failure begins. Damage due to compressive stresses is assumed to be negligible. Subsequently, the second stage, named the propagation of failure, takes place. Component failure occurs at the end of this stage when the total carrying capacity of the structure is expended. This methodology utilizes commercially available finite element packages and takes into account the time varying creep stress distributions (stress relaxation). The creep life of a component is divided into short time steps, during which, the stress distribution is assumed constant. The damage is calculated for each time step based on a modified Monkman-Grant creep rupture criterion. Failure is assumed to commence when the normalized accumulated damage at a point in the body is equal or greater than unity. For tensile/compressive stress states, rupture is assumed to take place when the damage zone is large enough so that the component is no longer able to sustain load. The corresponding time will be the creep rupture life for that component. Flexural and C-ring data of siliconized silicon carbide KX01 material are used to test the viability of this methodology. The NASA integrated design code CARES/*Creep* (Ceramics Analysis and Reliability Evaluation of Structures/*Creep*) which utilizes this damage accumulation model was used for this purpose. It was found that the methodology described in this paper yielded reasonable creep rupture life predictions given the amount of scatter in the data.

INTRODUCTION

Advanced structural ceramics are becoming viable materials for many high temperature applications including gasoline, diesel, and gas turbine engine components. Attractive properties such as low density, high strength, high stiffness, and corrosion resistance are allowing ceramics to supplant alloys in these demanding applications. The result is lower engine emissions, higher fuel efficiency, and optimized design.

The advent of new techniques in ceramic processing technology has yielded an improved class of ceramics that are highly resistant to creep at high temperatures (Ferber, et al., 1994, Ding, et al., 1994, Menon, et al., 1994a). Such desirable properties have generated interest in using ceramics for auxiliary power unit, and turbine engine component applications where the design lives for such systems are on the order of 10,000 to 30,000 hours. These long life requirements necessitate subjecting the components to relatively low stresses. The combination of high temperatures and low stresses typically places failure for monolithic ceramics in the creep rupture region of a time-temperature-failure mechanism map (Wiederhorn, et al., 1994, Quinn, 1990).

A previous paper published by the authors (Powers, et al., 1996) described a deterministic damage based approach and the structure of an integrated design code, named CARES/*Creep* (Ceramics Analysis and Reliability Evaluation of Structures/Creep), to predict the lifetimes of structural components subjected to sustained tensile stress states. This approach utilizes commercially available finite element packages and takes into account the time varying creep stress

Presented at the International Gas Turbine & Aeroengine Congress & Exhibition
Orlando, Florida — June 2–June 5, 1997

distribution (stress relaxation). In this approach the creep life of a component is discretized into short time steps, during which, the stress distribution is assumed constant. The damage is then calculated for each time step based on a creep rupture criterion. The creep rupture models used in the code are the Monkman-Grant (Monkman, et al., 1956), and the Modified Monkman-Grant criteria (Menon, et al., 1994b). Failure is assumed to occur when the normalized accumulated damage at any point in the component is greater than or equal to unity. The corresponding time will be the creep rupture life for that component. The success of this methodology was demonstrated for ceramic components subjected to creep conditions and nonuniform tensile multiaxial transient stress states (Powers, et al., 1996).

The methodology described above can be successful in predicting the creep lives for components subjected to multiaxial tensile or compressive stress states. However, this methodology in its present status can not be used to predict the creep rupture life for components subjected to simultaneous tensile and compressive stresses, especially for materials that display different tensile and compressive creep properties. Investigators found significant discrepancies between the creep lives of tensile and flexure specimens for both ceramic (Wiederhorn, et al., 1988, Chuang et al., 1988, Chuang et al., 1989, Chuang et al., 1991, Fields, et al., 1996, Wilkinson, et al., 1991) and metallic (Fairbrain, 1974) materials.

The objective of this paper is to describe an analytical methodology and to enhance the current version of the integrated design program CARES/*Creep* to include the prediction of lifetimes for ceramic structural components subjected to simultaneous tensile and compressive creep stress states. Flexural and compressed C-ring siliconized silicon carbide KX01 specimens tested in creep were utilized to examine the viability of this methodology (Wiederhorn, et al., 1988). These specimens were chosen because they display simultaneous nonuniform tensile and compressive stress fields. These stress fields will vary with time as the specimens creep. In addition, these specimens possess uniaxial stress states. Because only limited multiaxial ceramic creep data exists to guide the development of a proven multiaxial creep rupture criterion, the effect of creep multiaxiality was excluded from the life prediction methodology within this paper. The siliconized silicon carbide material KX01 was selected because the tensile, compressive, flexural, and C-ring creep data necessary to perform the finite element, and creep rupture analysis were available from the open literature (Wiederhorn, et al., 1988, Chuang, et al., 1989, Chuang, et al., 1991).

The CARES/*Creep* program is made up of two modules, and is currently customized to run as a post-processor to the ANSYS finite element code. The first module is a parameter estimation program used to compute the primary creep parameters based on the time hardening rule, the steady state parameters based on the Norton equation, and the creep rupture parameters based on the Monkman-Grant (MG) and the Modified Monkman-Grant (MMG) criteria. The second module, contains the coding for calculating the cumulative damage, and thus the creep rupture life for the component in question.

BACKGROUND

Engineers are generally interested in calculating the creep deformation and predicting the life for components subjected to creep conditions. Both endeavors, include the understanding of the creep and creep rupture mechanisms, the modeling of the material's creep behavior using appropriate constitutive equations, and subsequently choosing a rupture criterion suitable to that material. This section contains a brief literature review of these three topics.

Creep Damage in Ceramics Tested in Tension and Flexure

At high temperatures, creep deformation in ceramics can occur due to several competing mechanisms, depending on the stress and temperature levels. These mechanisms include diffusional creep, basal slip, grain boundary sliding, and cavitation. Cavitation was found to play an important role in the creep process of many ceramics, including AVCO and ARCO alumina (Wilkinson, et al., 1991), siliconized silicon carbide KX01 and SCRB210 (Wiederhorn, et al., 1988), and silicon nitride NT154 and PY6 (Luecke, et al., 1993, Menon, et al., 1994b, Ferber, et al., 1992). Fields (1996) suggests that due to such findings, creep in structural ceramics is primarily a consequence of cavity formation.

When ceramics are subjected to tensile loading at high temperatures, cavitation influences the creep process in several ways (Fields, et al., 1996). For the KX01 material, which will be used to demonstrate the life prediction methodology described in this paper, Carroll et al. (1988) found that creep strain was proportional to the volume fraction of cavities formed during creep. Another manifestation of cavitation is the asymmetric tensile/compressive creep behavior observed in ceramics (Morrell, et al., 1973, Wiederhorn, et al., 1988, Ferber, et al., 1990). For the same applied stress, tensile creep rates are often 10 to 100 times faster than compressive creep rates (Fields, et al., 1996). This increase in the tensile creep rate is related to the degree of cavitation because ceramics creep faster when cavities form. In compression, cavitation is hindered due to the compressive stress state. For example, in the KX01 material cavitation in compression does not occur at all (Hockey, et al., 1992). A third consequence of cavitation is the enhanced transient (time-dependent) stress distribution observed in flexural and C-ring specimens. As creep deformation takes place, the stress distribution relaxes at the tensile surface and increases at the compressive surface, thus insuring equilibrium. As a consequence, the neutral axis shifts closer to the compressive surface of the specimen.

Fields and Wiederhorn (1996) conducted creep testing in both tension and flexure on the KX01 material at 1300°C. Their experimental results indicated that the cavitation volume was proportional to the creep strain in both tension and flexure. They observed that at low strains, cavities nucleated at random throughout the test specimen, then coalesced to form cracks that eventually were the cause of failure. However, once cracks are nucleated, they evolved much differently in flexure bars than in tensile specimens. In tension, there is no stress relaxation and the rate of crack growth increases as they get longer. In contrast, stress relaxation due to cavitation on the tensile surface of the bend bar reduces the driving force for crack growth. As a result, cracks formed in flexure bars are more stable than those formed in tensile specimens. Fields and Wiederhorn further observed that many cracks can form in flexural specimens without causing them to fail. Because of such differences, the conditions for failure in tension and flexure are different. Failure strains in flexure for the KX01 material were found to be twice those in tension for the same stress and temperature (2% and 1%, respectively).

Wilkinson et al. (1991) conducted creep testing between 1200°C and 1250°C, using tensile and flexure specimens, on hot pressed fine grained (»1mm) alumina manufactured by ARCO. They also observed

that the lifetimes of bend bars are greater than those for tensile specimens. At intermediate stress levels, they found that this alumina material did not fail in flexure for strains up to 18%, while tensile specimens failed at strains between 8% and 10%. Further, they observed that the propagation of cracks controlled the final fracture process in both tension and flexure. In bending, extensive coalescence of microcracks on different planes took place through a shear band type process, hence enhancing the stress relaxation on the tensile surface. This, Wilkinson et al. stated, substantially increased the failure time of bend bars with respect to tensile specimens.

The discrepancy in the creep lives in tension and bending was also observed in metals. Fairbrain (1974) conducted creep tests in tension and cyclic bending on aluminum tubes. He used the reference stress approach to predict the creep behavior of components using tensile specimens. The reference stress method is based on the hypothesis that it is often possible to determine a stress, named the reference stress, at which the creep rate from a tensile specimen is proportional to a given component's (in this case, bend bar) displacement rate (for example, curvature). Fairbrain observed that fracture occurred in simple tension without any apparent cracking other than at the fracture. On the other hand, extensive cracking on the tensile surface along the full length of the bend tubes was visible. He explained this cracking pattern in the bend tubes to be a result of the relatively long time available for cracks to develop before failure. While cracks are forming in the regions of the tube subjected to the greatest tensile stresses, there remains a large volume of the tube subjected to low and compressive stresses which will not cause any cracking. Thus the cracking process in bending becomes much slower, more spread, and more stable process than in simple tension. Fairbrain's reference stress analytical approach resulted in fair predictions of bend creep behavior using tensile specimen data. However, his analysis was based on the assumptions that the material displays symmetric tension/compression creep behavior, which might be a reasonable assumption for metals but not for ceramics. Further, his analysis was based on stationary steady state creep conditions, and hence did not take into account the time varying stress state.

Creep Constitutive Relations

The creep strain curve resulting from a constant load test is a function of stress, temperature, and time. Several proposed constitutive relations are capable of simulating the entire creep curve (primary, secondary and tertiary). These laws include the theta projection method (Evans, et al., 1987, Maruyama, et. al., 1987), the continuum damage mechanics approach (Kachanov, 1960, Dunne, et al., 1990, Hayhurs, et al., 1975, Othman, et al., 1990), and the internal (back) stress model (White, et al., 1995, Brown, et al., 1989, Kraus, 1980).

Many types of ceramics, however, do not display tertiary creep behavior (Sundberg, et al., 1994, Cuccio, et al., 1995, Ohji, et al., 1993, Lewis, et al., 1992, Sankar, et al., 1994). Therefore, it is appropriate for creep analysis of ceramics to use constitutive equations describing only the primary and secondary creep regions. Many formulas, and combinations of these formulas exist for such formulation. One of these constitutive laws is known as the Baily-Norton time hardening rule (Kraus, 1980, Norton, 1929, Boyle and Spence, 1983) and is given by the following equation:

$$\dot{\varepsilon} = a_1 \sigma^{a_2} t^{a_3} \exp\left[-\frac{Q}{RT}\right] \tag{1}$$

where $\dot{\varepsilon}$ is the creep strain rate, σ, t, and T are the stress, time, and absolute temperature. The material constants a_1, a_2, a_3, and Q are determined from experiments and R is the universal gas constant. The Baily-Norton constitutive law was selected to describe the creep behavior of ceramics in the CARES/*Creep* code, because of its widespread use, and success in fitting the creep data as a function of stress, temperature, and time. Furthermore, this relationship, in association with Prandtl-Reuss plasticity flow rule, satisfies four basic requirements for multiaxial creep analysis (Kraus, 1980). These requirements are: 1) the multiaxial formulation must reduce to the uniaxial formulation when appropriate, 2) the model contains constancy of volume for creep conditions, 3) the model reflects lack of influence of hydrostatic stress, and 4) principal directions of stress and strain coincide. The constancy of volume requirement is a result of the original development of this theory for metals. Ceramics contain voids which expand under creep conditions. A theory incorporating this phenomena is not yet available for finite element calculations.

Creep Rupture

The majority of current engineering design methodologies against creep, fit into four major categories. The first is graphical, where the time to reach a given strain, or fracture, at a given stress or temperature is obtained from a creep life diagram. Some of the techniques that belong to this group are the Larson-Miller (Larson and Miller, 1952), Sherby-Dorn (Orr, et al., 1954), minimum commitment (Manson, et al., 1971), Quinn (1986), and Jones (1986) methods. These approaches utilize parameters which when plotted against stress would yield unique curves that can be used to predict the life of components subjected to creep rupture loading.

The second category includes analytical methods to predict the creep life for structural components. The Monkman-Grant (MG) method (Monkman and Grant, 1956) is one of the most utilized approaches for ceramics and is based on a power relation between time to failure and steady-state creep rate given by the following equation:

$$\dot{\varepsilon}^{b_2} t_f = b_1 \tag{2}$$

here t_f is the time to failure and b_1 and b_2 are constants. The above equation assumes that a unique curve can describe failure for a given material independent of temperature. This assumption was found to be invalid for some ceramic materials (Ferber, et al., 1992, Luecke, et al., 1993, Menon, et al., 1994a), which displayed stratification of the MG curve depending on the temperature level. Thus, a modified Monkman-Grant (MMG) equation was introduced (Menon, et al., 1994b) to take the temperature into account and is given by the following formula:

$$\ln t_f = d_1 - d_2 \ln \dot{\varepsilon} + \frac{d_3}{T} \tag{3}$$

where d_1, d_2 and d_3 are constants. The MG and the MMG criteria were found to be very successful in describing the creep rupture behavior for ceramics, and thus are used heavily in the ceramics literature. For this reason, these criteria were selected as the basis for predicting the creep life of ceramic components in the CARES/*Creep* code. Note that the MMG criterion collapses to the MG criterion when d_3 is set equal to zero.

Differential formulations constitute the models making up the third category of approaches for creep rupture prediction. Continuum damage mechanics , and internal (back) stress concepts belong to this

category.

Probabilistic formulations make up the fourth category for creep rupture life prediction (Lange, 1976, Duffy and Gyekenyesi, 1989). Currently, most ceramic researchers utilize deterministic approaches to describe the creep deformation, and to even predict the creep rupture lives for ceramics. Ceramic creep deformation, and thus creep parameters, display less stochastic and more deterministic behavior compared to fast fracture and slow crack growth failure data. An indication of that is the absence of the so called "size effect" (Wiederhorn, et al., 1994) in some ceramics, which is a characteristic of the probabilistic behavior of brittle fracture in ceramics.

A probabilistic creep theory is not well developed at this point. The CARES/*Creep* code utilizes a deterministic approach at this time to predict the creep life. Incorporating probabilistic creep life prediction is, however, planned for future enhancements of the code.

THEORY

The creep response of a ceramic component must be evaluated in order to determine its service life. The life of a component is determined by calculating the damage over time. The creep response for a given component can be divided into two categories: evaluating the creep deformation parameters for a given constitutive creep relationship and assessing the creep rupture life of the component.

Creep Constitutive Relations

The creep curve is broken up into three stages: primary, secondary and tertiary. The equations for this curve were formulated to match the creep models built into ANSYS. The tertiary stage is not included in the analysis since it implies impending failure and because many ceramics do not exhibit such behavior. ANSYS contains a library of strain rate equations characteristic of materials being used in creep design applications. The creep strain rates for primary and secondary creep are a function of stress, time, and temperature.

ANSYS does not divide creep into unique stages as is done in conventional creep curves. Both primary and secondary creep are assumed to be in effect simultaneously. Thus, the material constants for these relations must be computed so to account for this type of loading. The total creep strain is given by

$$\varepsilon_{cr} = \varepsilon_p + \varepsilon_s \tag{4}$$

where ε_p is the primary and ε_s is the secondary components of creep strain. The primary creep strain rate is given as

$$\dot{\varepsilon}_p = C_1 \sigma^{C_2} t^{C_3} \exp\left[-\frac{C_4}{T}\right] \tag{5}$$

The secondary creep strain rate is given by

$$\dot{\varepsilon}_s = C_7 \sigma^{C_8} \exp\left[-\frac{C_{10}}{T}\right] \tag{6}$$

where C_i are material parameters determined from creep experiments. These constants are not numbered sequentially since i is the location of the value in the ANSYS data table. The procedure for calculating the creep parameters, C_1, C_2, C_3, C_4, C_7, C_8, and C_{10} is described in Powers, et al. (1996).

Life Prediction Based On Damage Initiation

Due to stress redistribution during creep loading conditions, the steady state (secondary) creep rate, $\dot{\varepsilon}_s$, also varies with time. Therefore, the MG failure criterion may not be used in the form given for equations (2) and (3) to predict the lifetime. The following concept, based on damage accumulation, can be used to predict the service life using the MG criterion.

The component's predicted life is determined based on a damage function, D. The damage function is generally defined as

$$0 \le D \le 1$$

where D=0 for an undamaged component and D=1 for a failed component. If failure is assumed to occur at time, $t=t_f$, then the damage, D, is equal to unity at that time. A nonlinear analysis divides the time into steps over which the stress and strain rates are assumed to be constant. The cumulative damage is subsequently calculated as time elapses in a manner similar to Miner's rule for fatigue loading. The damage is expressed as

$$D = \frac{\Delta t_1}{t_{f1}} + \frac{\Delta t_2}{t_{f2}} + \ldots + \frac{\Delta t_n}{t_{fn}} = \sum_{i=1}^{n} \frac{\Delta t_i}{t_{fi}} \tag{7}$$

where t_{fi} is the creep rupture time based on the loading conditions during the i-th time step, Δt_i is the duration of the i-th time step, and n is the number of time steps to failure.

The creep rupture time for the i-th time step, t_{fi}, is determined using an appropriate failure criterion. For the MG criterion given in equation (2), this time is

$$t_{fi} = \frac{b_1}{\dot{\varepsilon}_i^{b_2}} \tag{8}$$

where $\dot{\varepsilon}_i$ is the secondary creep strain rate for the i-th time step. Substituting the secondary creep strain rate into equation (8) yields

$$t_{fi} = \frac{b_1}{\left[C_7\, \sigma_i^{C_8} \exp\left(-\frac{C_{10}}{T_i}\right)\right]^{b_2}} \tag{9}$$

where σ_i and T_i are the stress and temperature of the i-th time step. Substituting equation (9) into equation (7) gives an expression for the damage

$$D = \frac{C_7^{b_2}}{b_1} \sum_{i=1}^{n} \sigma_i^{b_2 C_8} \exp\left[-\frac{b_2 C_{10}}{T_i}\right] \Delta t_i \tag{10}$$

In this methodology, failure is assumed to occur when the normalized cumulative damage at any point in the component reaches unity. The corresponding time will be the creep rupture life for that component.

The modified Monkman-Grant (MMG) criterion may also be applied to compute the damage. Substituting the secondary creep strain rate into equation (3) yields

$$t_{fi} = C_7^{-d_2}\, \sigma_i^{-d_2 C_8} \exp\left[d_1 + \frac{d_2 C_{10}}{T_i} + \frac{d_3}{T_i}\right] \tag{11}$$

Substituting equation (11) into equation (7) gives an expression for the damage

$$D = C_7^{d_2} \sum_{i=1}^{n} \exp -\left[d_1 + \frac{d_2 C_{10}}{T_i} + \frac{d_3}{T_i}\right] \sigma_i^{d_2 C_8}\, \Delta t_i \tag{12}$$

Failure is again assumed to occur when the normalized cumulative damage at any point in the component reaches unity.

Life Prediction Based on Damage Initiation and Propagation

The methodology described in the previous section can lead to very conservative estimate for the lives of components subjected to

creep conditions. This is because it was assumed that failure due to creep rupture occurs when the damage reaches unity at any point in the component. Kachanov (1960) referred to this time period as the stage of latent failure, t_1, and Johnson called it the incubation period (Odqvist, 1974). In general, for ceramics final creep failure occurs due to cavitation and damage propagation. Hence, the assumption that failure occurs at t_1, indicates that failure takes place when the damage zone is infinitesimally small. Such a statement may be valid for components subjected to relatively uniform tensile stress distributions.

For cases when decaying tensile or simultaneous tensile/compressive stress distributions exist, this methodology should be modified to take into account the additional time spent for the damage zone to travel through the specimen. This time duration represents the second stage of failure and is referred to as the stage of damage propagation, t_2. This stage ends with the final rupture of the component. Hence, the final rupture time (lifetime), t_R, is given by:

$$t_R = t_1 + t_2 \tag{13}$$

The incubation period, t_1, is calculated as was described in the previous section. Namely, t_1 corresponds to the time it takes the damage, as defined by equations (10) and (12), to reach unity at any point in the component. The methodology to calculate the failure propagation period, t_2, will be described next.

The method by which the failure propagation period is determined will be a function of the non-homogeneous stress state. Cohrt, et al., (1984) observed that for materials exhibiting asymmetric creep, the bending creep test does not illustrate the behavior of the outer fibers, but reveals the creep behavior of the bulk of the bending beam, thus representing the contribution of the entire specimen.

During the propagation stage, a damage front defined by the condition D=1 will travel through the body or surface of the component. Component failure occurs at the end of this stage when its total load carrying capacity is exceeded. The corresponding time will be the creep rupture life of the component. The size of the critical damage zone for creep rupture failure varies depending on the load conditions and component configuration. One estimate for the duration of the propagation stage is to assume it equal to the time it takes for the damage zone to penetrate the initial tensile stressed portion of the structure.

PROGRAM CAPABILITY

The CARES/*Creep* integrated design computer program predicts the service life of a monolithic ceramic component as a function of its geometry and loading conditions. CARES/*Creep* couples commercially available finite element programs, with the design methodology presented above to predict the creep life of a component. The code is divided into two separately executable modules, CARES/CRPEST and CARES/*Creep*, which perform: (1) calculation of creep and creep rupture parameters from experimental data using laboratory specimens; and (2) damage evaluation, and life prediction of thermo-mechanically loaded ceramic components, respectively. Finite element heat transfer and nonlinear stress analyses are used to determine the transient temperature and stress distributions in the component. The creep life of a component is discretized into short time steps, during which, the stress, temperature, and strain distributions are assumed constant. The damage, failure propagation, and life are calculated as described above. CARES/*Creep* produces a cumulative damage plot for graphical rendering of the structure's critical regions. Such plots can then be used by engineers to redesign or optimize the component as needed.

A schematic representation of the integrated design process used in CARES/*Creep* is shown in Figure 1. The CARES/*Creep* algorithm makes use of the nonlinear stress analysis capabilities of the ANSYS finite element program. Before building a model in ANSYS, the creep response of the material must be known. An input file containing these parameters is generated by the parameter estimation module of CARES/CRPEST. This module is written in FORTRAN 77 and has as its input, data from creep tests. After the parameter estimation and the FEM nonlinear analysis has been completed, the second half of the CARES/*Creep* program may be run. This module is executed from within the ANSYS program and is written in APDL (ANSYS Parametric Design Language). APDL routines usually take the form of an ANSYS macro which is a sequence of ANSYS commands recorded on a file for repeated use. By recording these commands on a macro, they can be executed with one ANSYS command. When this execution is completed, a damage map of the component is displayed in the graphics window. This map consists of a contour plot of the component's damage at the time when failure has taken place, or at any service life desired by the engineer.

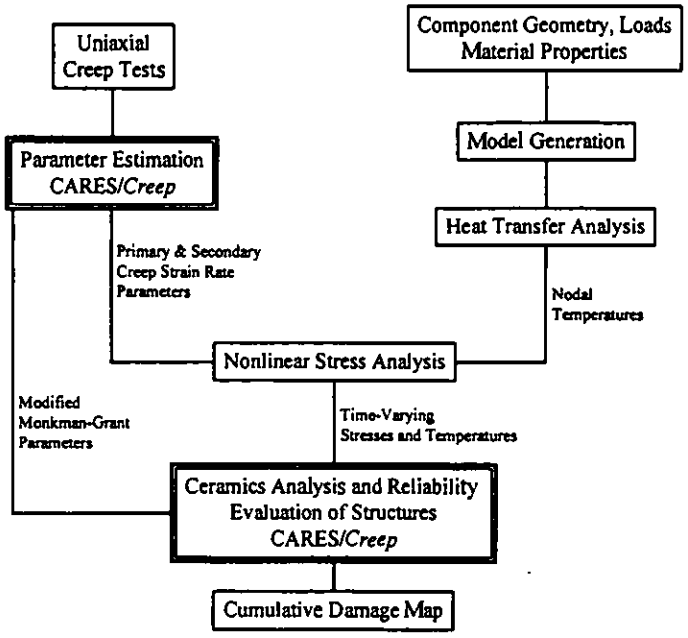

Figure 1 Block diagram for the analysis of a monolithic ceramic components using CARES/*Creep*.

The parameter estimation module computes the Norton, Bailey-Norton, MG, and MMG parameters from uniaxial creep tests. Experimental data may be in one of two forms. The first is the more complete set of data which includes the strain versus time for all stress and temperature specimen data. The second data option available yields secondary creep, MG, and MMG parameters. For this data set the minimum strain rate (secondary creep strain rate) versus time to failure are input for all stress and temperature conditions.

As was stated earlier, ceramics display asymmetric creep behavior since their tensile and compressive creep properties differ. In ANSYS,

the laws available within the standard creep tables assume symmetric creep behavior. Fortunately, the ANSYS FEM program offers an open architecture which allows linking of user supplied FORTRAN subroutines. Several User Programmable Features (UPFs) are currently available. One of these is the creep subroutine, allowing the user to specify any creep law that models the material at hand. This creep subroutine was used to install into ANSYS the asymmetric secondary creep laws describing the KX01 material behavior. These laws are described in the section titled Creep and Creep Rupture Properties of the KX01 Material.

The user subroutine for creep is accessed by setting the constant C_6 in the creep data table equal to 100. When this is done, the ANSYS program will call the creep subroutine written by the user. This assumes that the version of ANSYS currently being executed has the appropriate subroutines compiled and linked to the ANSYS program.

CARES/*Creep* is an ANSYS postprocessor code which computes the damage for each element as described in the theory section. Finite element analysis is an ideal mechanism for obtaining the stress distribution needed to calculate the service life of a structure. Each element can be made arbitrarily small, such that the stresses can be taken as constant throughout each element (or subelement). In CARES/*Creep*, the damage calculations are performed at the element centroid, or optionally, at the node points. Using the nodal points enables the element to be divided into sub-elements, where the stresses and temperatures are calculated.

EXAMPLES

Two examples are presented to demonstrate the methodology discussed in this paper for predicting the creep rupture life of ceramic components subjected to simultaneous tensile/compressive loading. The first example is the creep life prediction of flexure bars subjected to four point bending. The second example is the creep life prediction of C-ring specimens subjected to compressive diametral loading. Experimental flexure, C-ring, tensile, and compressive creep and creep rupture data for the KX01 material were obtained from the open literature. This material's creep and creep rupture properties are presented. The creep rupture lives for the flexure and C-ring specimens were predicted using the tensile and compressive creep and creep rupture properties. These predicted lives were then compared to the experimental ones.

Creep and Creep Rupture Properties of the KX01 Material

Wiederhorn et al. (1988) conducted creep testing on KX01 siliconized silicon carbide material at 1300°C using flexure, C-ring, tensile and compressive specimens. The KX01 material is a two-phase composite fabricated by the infiltration of silicon metal into a porous silicon carbide preform. The composite contains 33 vol % silicon metal embedded with 3-5 mm SiC particulates.

The primary and tertiary stages of the creep tensile and compressive curves for the KX01 material were found to be minimal (Wiederhorn et al., 1988). Most of the creep lives of the specimens were in the secondary creep stage. Further, they found the KX01 material to display significant asymmetric creep behavior. Figure 2, Wiederhorn, et al., 1988, shows the discrepancy between the tensile and compressive, and the bilinear creep rate behavior as a function of stress at 1300°C for the KX01 material. In both tension and compression, the creep rate displayed a bilinear power (Norton) law behavior with a transition point at a threshold stress. This threshold stress was determined to be 100 MPa in tension and 200 MPa in compression. The stress exponents were approximately 4 for low strain rates, and 10 for high strain rates.

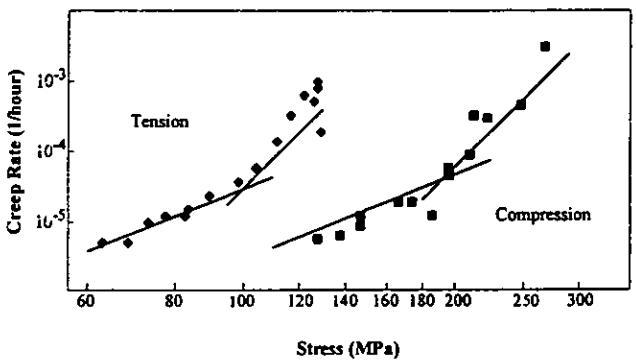

Figure 2 Creep rate vs. stress for the siliconized silicon carbide material tested in tension and compression (Wiederhorn, et al., 1988).

In tension, the following equations describe the bilinear creep rate (Chuang, et al., 1989): For $\sigma_a > \sigma_0$,

$$\dot{\varepsilon}_s = \dot{\varepsilon}_0 \left(\frac{\sigma_a}{\sigma_0} \right)^N \tag{17a}$$

and for $0 \le \sigma_a \le \sigma_0$,

$$\dot{\varepsilon}_s = \dot{\varepsilon}_0 \left(\frac{\sigma_a}{\sigma_0} \right)^n \tag{17b}$$

where σ_a is the applied stress; σ_0 is the threshold stress for damage; $\dot{\varepsilon}_0$ is the creep rate at $\sigma_a = \sigma_0$, N is the stress exponent in the high stress regime, n is the stress exponent in the low stress regime.

In compression, the following similar set of equations are applicable (Chuang, et al., 1989): For $\sigma_a < -\beta\sigma_0$,

$$|\dot{\varepsilon}_s| = \lambda |\dot{\varepsilon}_0| \left(\frac{|\sigma_a|}{\beta\sigma_0} \right)^N \tag{18a}$$

and for $-\beta\sigma_0 \le \sigma_a \le 0$,

$$|\dot{\varepsilon}_s| = \lambda |\dot{\varepsilon}_0| \left(\frac{|\sigma_a|}{\sigma_0} \right)^n \tag{18b}$$

where β and λ are the ratios of compressive to tensile stress threshold, and creep rates, respectively. The values for these parameters were computed to be: $\dot{\varepsilon}_0 = 2.88 \times 10^{-5}$ 1/hr, σ_0=100 MPa, λ= 0.1, N = 10, n=4, and β=2. These creep equations were programmed into ANSYS using the user creep subroutine described in the previous section..

The KX01 material was found to obey the MG creep rupture criterion as described in equation (2) and the parameters $b_1 = 0.001211/\text{hr}^{0.2}$, and b_2=1.2 (Chuang, et al., 1989).

Flexure Bar

This example demonstrates the use of the CARES/*Creep* code to predict the time-dependent behavior of ceramic components subjected to simultaneous tensile/compressive creep conditions. Wiederhorn et al. (1988) tested KX01 flexure specimens, 50 mm x 4 mm x 3 mm in four point bending with inner and outer loading spans of 10 and 40 mm, respectively. Tests were conducted at 1300°C.

The FEM mesh for the bend specimen is shown in Figure 3. The meshed model contains 1200 eight node quadrilateral elements (PLANE82), and takes advantage of symmetry by modeling half the bend bar. The applied loads were placed as point loads, while the reactions were applied by restraining the displacements at the supports.

Figure 3 Finite element mesh for the 4-pt bend specimen.

Figures 4a and 4b display the elastic stress distribution at t=0 corresponding to an initial tensile stress of 250 MPa for the bend specimen and t=14.5 hours corresponding to the time when the damage first reached unity. It is apparent from these figures that due to creep deformation, the outer fiber tensile stress relaxed from 250 MPa at t=0, to about 125 MPa at t=14.5 hours and beyond. The stress distribution in the bend bar converged to its stationary value ten hours after the load was applied. These figures also show how the neutral axis shifts towards the compressive region as the specimen creeps.

Figure 4 Stress distribution in the 4-pt bend specimen at time equal to a) zero and b) t_1 hours, where the maximum tensile stress is 250 and 125 MPa, respectively.

The FEM flexure bar creep stress analysis was checked against closed form solutions for two limiting bend bar cases. The first case represents the stationary stress distribution in a homogeneous (similar tensile and compressive creep properties) beam with depth W as a function of position y (Timoshenko, 1968):

$$\sigma(y) = \sigma_{el,max} \frac{2n+1}{3n} \left(\frac{2y}{W}\right)^{1/n} \tag{16}$$

where, $\sigma_{el,max}$ is the elastic maximum stress, and n is the Norton creep stress exponent. The second case against which the FEM creep analysis was checked was for the stationary stress distribution in a beam with asymmetric creep behavior. The stationary tensile, $\sigma_T(y)$, and compressive, $\sigma_C(y)$, stress distributions in a bend bar are given by (Cohrt, et al., 1984):

$$\sigma_T(y) = \sigma_{el,max} \frac{2n+1}{6n} \left(1 + S^{n/(n+1)}\right) \left(\frac{y}{W_T}\right)^{1/n} \tag{17a}$$

$$\sigma_C(y) = \sigma_{el,max} \frac{2n+1}{6n} \left(1 + S^{n/(n+1)}\right) \left(\frac{y}{W_C}\right)^{1/n} \tag{17b}$$

$$\frac{W_T}{W_C} = S^{n/n+1} \tag{18}$$

where $S=\sigma_T/\sigma_C$ is the ratio between the applied stresses, for the same creep rate, in compression and tension, W_T and W_C are the depths of the tensile and compressive portions of the beam when the stationary creep state is reached, respectively. Obviously, $W_T+W_C=W$. For both limiting cases, the FEM solution converged to the stationary creep stress distributions (corresponding to long creep duration) given by equations (16) and (17).

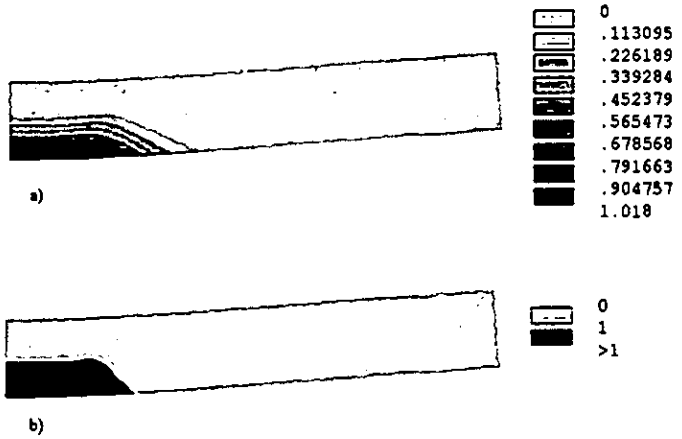

Figure 5 Cumulative damage in the 4-pt bend specimen at a) time equal to t_1 and b) time equal t_u.

Figure 5a and 5b show the damage maps for the flexure specimen tested at 250 MPa (elastic maximum stress), at t=14.5 hours corresponding to the time when the damage first reached unity and at t=80 hours corresponding to the time where predicted rupture occurs. Such damage maps can help the designer identify the critical regions where failure is most probable to occur.

Figure 5a shows the damage zone corresponding to the time when the damage first reaches unity, $t=t_1$. As can be seen in the figure, the damage zone is the thin layer located at the outer tensile fiber between the two inner loads. Figure 5b shows the damage zone defined by the condition $D \geq 1$. In this analysis, it was assumed that failure would occur when the initial portion of the bend beam under

tension (half the depth) is damaged. This assumption is in accordance with that suggested by Odqvist (1974) for metals. Hence, figure 5b which shows the damage zone defined by D=1 expanded to cover the portion of the beam initially stressed in tension, corresponds to the rupture time, t_R, at the end of the damage initiation and propagation stages.

Table 1 lists the experimental rupture lives, the predicted lives corresponding to the end of the latent stage of failure (t_I), and the predicted rupture lives (t_R) corresponding to the end of the failure propagation stage for four bend bars. As can be seen from the table, the methodology described in this paper resulted in conservative estimates for creep rupture lives of the bend bars if the value of t_I is used for predicted life. When initiation and propagation damage stages were to be considered, this methodology resulted in excellent agreement with experimental results.

Table 1. Experimental and predicted creep lives for KX01 siliconized silicon carbide bend bars subjected to four point bend loading at 1300°C.

Applied Stress (MPa)	Experimental Failure Time (hours)	t_I (hours)	Predicted Rupture Life, t_R (hours)
200 / 100*	830	200	830
250 / 125	55	14.5	80
300 / 150	12	1.2	8.6
350 / 175	1.3	0.12	1.3

* Maximum tensile stress values for elastic/steady state conditions

C-ring Subjected to Diametral Compression

In this example the CARES/*Creep* code is used to predict the creep rupture lives of C-ring specimens subjected to diametral compression. Chuang et al. (1991) conducted creep and creep rupture testing for the KX01 material using C-ring specimens at 1300°C. Chuang et al. (1991) developed an analytical model and performed FEM studies (Chuang, et al., 1992) describing the stress distribution and deformation as a function of time for compressed C-ring specimens subjected to creep conditions. However, these studies did not include a formulation for predicting the life due to creep rupture. Jadaan et al. performed analytical, FEM, and experimental studies to examine the fast fracture and slow crack growth behavior of tubular components using the C-ring specimen geometry (Jadaan, et al., 1991, Shelleman, et al., 1991, Jadaan, et al., 1993, Jadaan, et al., 1995).

The two dimensional FEM mesh for one of the six C-ring specimens examined in this paper is shown in Figure 6. This particular specimen was subjected to a constant compressive load of 106.4 N which resulted in a maximum tensile stress of 172 MPa and failed after 243 hours. The C-ring had a width B=6.3 mm, inner radius R_i=16 mm, and an outer radius R_o=19.05 mm. The meshed model contains 1386 eight node quadrilateral elements (PLANE82), and takes advantage of symmetry by modeling half the C-ring. The element distribution in the model was selected such that more elements were placed in the higher stressed region (near the apex). The applied loads were placed as point loads, while boundary conditions of symmetry, preventing displacement in the vertical direction while allowing displacement along the horizontal direction (rollers), were applied along the apex. To prevent rigid body motion, the node along the plane of the load at the inner surface of the C-ring was pinned, thus preventing displacement along the horizontal directions.

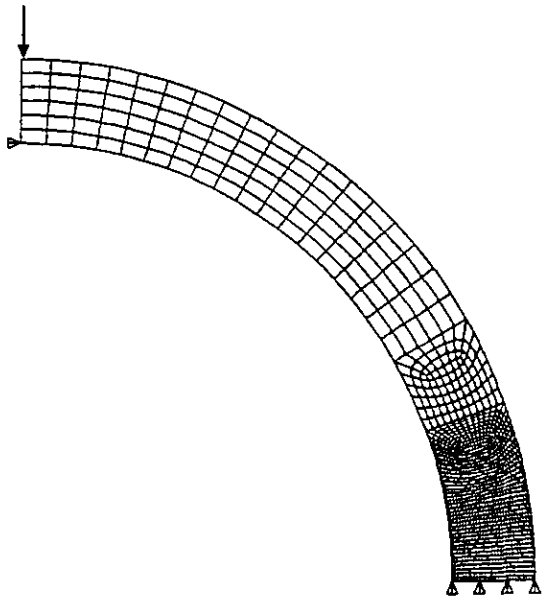

Figure 6 Finite element mesh for the C-ring.

Figures 7a and 7b display the stress distribution at t=0 for the C-ring specimen stressed to 172 MPa and t=390 hours corresponding to the time when the damage first reached unity, respectively. It is apparent from these figures that due to creep deformation, the outer fiber tensile stress along the apex relaxed from 172 MPa at t=0, to 96 MPa at t=390 hours. The stress distribution converged to its stationary value about 20 hours after the load was applied. These figures also show how the neutral axis shifts towards the compressive region as the specimen creeps. This FEM C-ring creep stress analysis was compared to a similar FEM analysis conducted by Chuang et al. (1992) and was found to be almost identical.

Figures 8a and 8b show the damage maps for the C-ring tested at 172 MPa initially, at t=390 hours corresponding to the time when the damage first reached unity, $t=t_I$, and at t=1400 hours corresponding to the time when predicted rupture occurs. Figure 8a shows the damage zone corresponding to the time when the damage first reaches unity, $t=t_I$. As can be seen in the figure, the damage zone is located at the outer tensile surface of the apex. Figure 8b shows the damage zone defined by the condition $D \geq 1$. In this analysis, it was assumed that failure would occur when the initial portion of the C-ring's apex under tension (half the depth) is damaged. Hence, figure 8b which shows the damage zone defined by D=1 expanded to cover the portion of the C-ring initially stressed in tension, corresponds to the rupture time, t_R, at the end of the damage initiation and propagation stages.

Table 2 lists the experimental rupture lives, the predicted lives corresponding to the end of the latent stage of failure (t_I), and the predicted rupture lives (t_R) corresponding to the end of the failure propagation stage for six C-ring specimens.

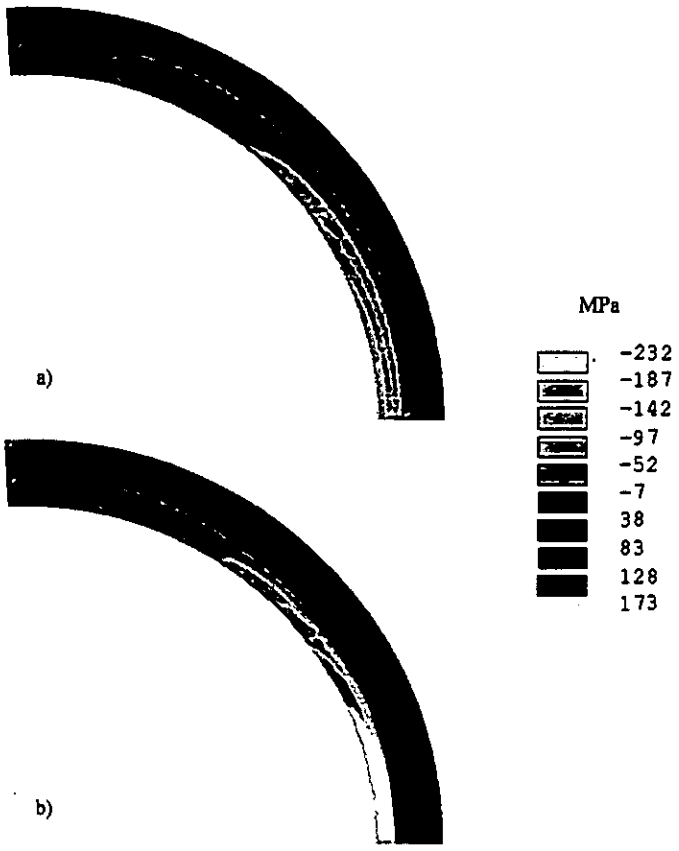

Figure 7 Tangential stress distribution in the C-ring at time equal to a) zero and b) t_1 hours, where the maximum tensile stress is 172 and 96 MPa, respectively.

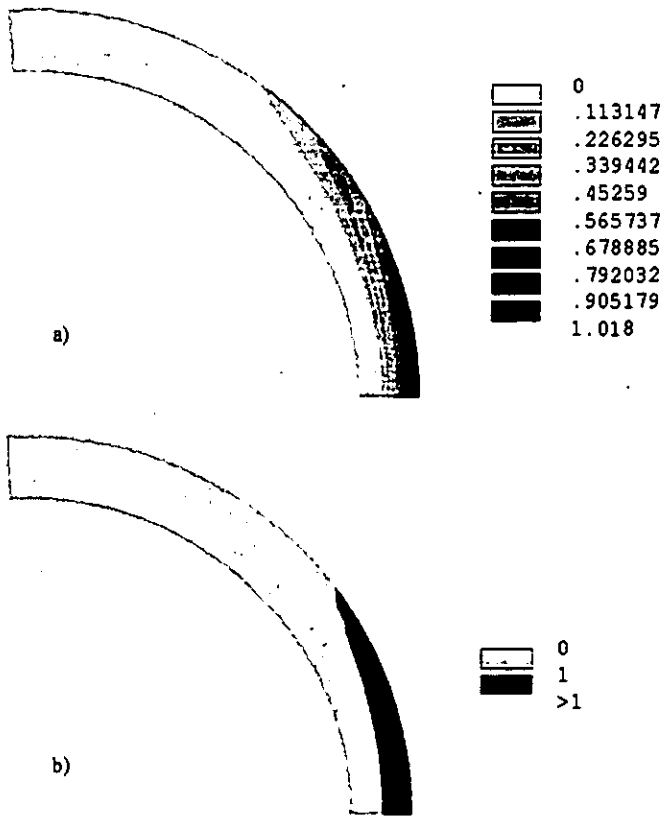

Figure 8 Cumulative damage in the C-ring at a) time equal to t_1 and b) time equal to t_R.

It is clear from Table 2 that the predicted rupture lives for the six tested C-ring specimens were longer than the experimental measurements. In addition, the predicted lives for the C-rings were less accurate than those for the bend bars listed in Table 1. It was expected that the C-rings would display similar creep rupture behavior to the bend bars since the compressed C-ring geometry is nothing but a curved beam. However, upon comparing the experimental creep rupture lives for C-rings and bend bars it is observed that given similar stress levels, the C-rings failed faster than the flexure specimens. For example, the 250 MPa stressed bend bar failed after 55 hours, while it took only 72 hours to rupture a C-ring stressed at the significantly lower stress of 182 MPa. To emphasize this point even further, note that the 200 MPa stressed bar failed after 830 hours.

Table 2 also highlights an important point about the nature of data scatter in ceramic creep rupture lives. This point becomes clear when the rupture lives for the 172 MPa (243 hours) and the 173 MPa (558 hours) are compared. Ceramics have been observed to display significant scatter in their creep rupture lives (Khandelwal, et al., 1995). This behavior underscores the importance of developing a probabilistic creep life prediction methodology for ceramic components. A manifestation of this scatter in the creep rupture data can also be seen by examining the creep lives for the last four C-rings listed in Table 2. For these specimens, the experimental data seems to suggest that as the applied stress increases, the creep rupture life increases accordingly. This trend, captured by these few data points, is obviously not correct but is a result of the scatter in data, and not having enough specimens tested. The creep life prediction theory presented in this paper is consistent, in that it predicts longer lives for lower applied stresses. This is apparent upon comparing the C-ring and bend bar predicted creep rupture lives as a function of applied stress. A probabilistic methodology should ultimately be utilized to predict the creep rupture lives of ceramics.

Table 2. Experimental and predicted creep lives for KX01 siliconized silicon carbide C-ring specimens at 1300°C.

Applied Stress (MPa)	Experimental Failure Time (hours)	t_1 (hours)	Predicted Rupture Life (t_R) (hours)
172 / 96*	243.3	390	1400
173 / 96	558	390	1375
182 / 101	71.7	280	1025
192 / 104	74.5	190	730
195 / 105	90.2	170	650
220 / 118	109	40	200

* Maximum tensile stress values for elastic/steady state conditions

One explanation of why the C-rings displayed shorter lives compared to the bend bars could be related to the difference in their surface finish. The C-rings were cut from tubes and were creep tested as is, without polishing the surfaces were damage would initiate. On the other hand the bend bars were polished resulting in smooth surface finish. This explanation seems consistent with the fact that the C-rings displayed shorter lives than the bend bars.

Tables 1 and 2 list the maximum tensile stresses corresponding to the initial elastic, and stationary stress states. For the bend bars and C-rings, the stationary maximum tensile stress ,occurring at the outer fiber, relaxed to about 50% and 55% of the initial elastic stress value, respectively. These similar ratios for the bend bars and C-rings show the analogous creep behavior between these two similar geometries, as expected.

Several advantages are apparent for the creep rupture life methodology presented in this paper. First, this methodology yields a cumulative damage map for the component showing the predicted failure location. This capability is very helpful for practical design applications. viewing of such damage maps, the user can change the design parameters to reduce the damage at the critical locations and optimize the design. In general for creep type loading applications, it is not a trivial task to predict the location of failure since the stress varies with time. Thus, failure will not necessarily occur at the location where stresses were highest at the beginning of loading, but can take place elsewhere as the stress components are redistributed. Second, this design methodology is capable of incorporating the primary creep strain effect into the analysis which could predict shorter lives (conservative predictions) than if only the secondary creep stain effect is used. Third, any creep rupture criterion (Larson-Miller, minimum commitment method,..etc.) can be utilized to compute the damage and predict the creep rupture life.

CONCLUSIONS

A general purpose creep life prediction code, CARES/*Creep*, has been developed, which is integrated with ANSYS finite element software, and can be used to predict the creep rupture life of ceramic components. In this paper, CARES/*Creep* was enhanced to predict the creep rupture lives of components subjected to highly nonuniform, and tensile/compressive stress fields. The creep rupture life is computed based on damage accumulation and is divided into two stages, the latent (incubation) stage of failure, and the damage propagation stage. Damage accumulation is calculated using the Monkman-Grant or the modified Monkman-Grant failure criteria. This methodology takes into account the transient nature of the stress state, and is capable of predicting the location of failure corresponding to the location of maximum damage. This approach also yields a damage map which can be used to redesign the component. It was concluded that the methodology described in this paper yielded reasonable creep rupture life predictions given the scatter in the data, and that the data used to carry out the analysis should be compatible with the loading conditions (stress, temperature, surface finish) that a given component sees in service.

REFERENCES

Brown, S., Kim, K., and Anand, L., 1989, "An Intemal Variable Constitutive Model for Hot Working of Metals," *International Journal of Plasticity*, Vol 5, pp. 85-130.

Boyle, J., and Spence, J., 1983, *Stress Analysis for Creep*, Butterworth & Co., London.

Carroll, D. F., and Tressler, R. E., 1988, "Accumulation of Creep damage in a Siliconized Silicon Carbide," *Journal of the American Ceramic Society*, Vol. 71, No. 6, pp. 472-477.

Chuang, T.-J., and Wiederhorn, S. M., 1988, " Damage Enhanced Creep in a Siliconized Silicon Carbide: Mechanics of Deformation," *Journal of American Ceramic Society*, Vol. 71, pp. 595-601.

Chuang, T.-J., Carroll, D. F., and Wiederhorn, S. M., 1989, "Creep rupture of a Metal-Ceramic Particulate Composite," *Advances in Fracture Research*, Proceedings of the 7th International Conference on Fracture, Houston, Texas.

Chuang, T.-J., Wei-Jun Liu, and Wiederhorn, S. M., 1991, "Steady-State Creep Behavior of Si-SiC C-rings," *Journal of American Ceramic Society*, Vol. 74, No. 10, pp. 2531-2537.

Chuang, T-J., Wang, Z.-D., and Wu, D., 1992, "Analysis of Creep in a Si-SiC C-Ring by Finite Element Method," Journal of Engineering Materials and Technology, Vol. 114, pp. 311-316.

Cohrt, H., Grathwohl, G., and Thummler, F., 1984, "Non-Stationary Stress Distribution in a Ceramic Bending Beam During Constant Load Creep," *Res Mechanica*, Vol. 10, pp. 55-71.

Cuccio, J, Brehm, P., Fang, H., Hartman, J., Meade, W., Menon, M., Peralta, A., Song, J., Strangman, T., Wade, J., Wimmer, J., and Wu., D., 1995, "Life Prediction Methodology for Ceramic Components of Advanced Heat Engines, Phase I." Oak Ridge National Lab., ORNL/Sub/89-SC674/1/V1.

Ding, J.-L., Liu, K. C., More, K. L., and Brinkman, C. R., 1994, "Creep and Creep Rupture of an Advanced Silicon Nitride Ceramic," *Journal of the American Ceramic Society*, Vol. 77, pp. 867-874.

Duffy, S. F., and Gyekenyesi, J. P., 1989, "Time Dependent Reliability Model Incorporating Continuum Damage Mechanics for High-Temperature Ceramics," NASA TM-102046.

Dunne, F., Othman, A., Hall, F., and Hayhurst, D., 1990, "Representation of Uniaxial Creep Curves Using Continuum Damage Mechanics," *International Journal of Mech. Science*, Vol. 32, No. 11, pp. 945-957.

Evans, R., Murakami, T., and Wilshire, B., 1987, "The Generation of Long-Term Creep Data for Silicon Nitride Ceramics," *British Ceramics proceedings*, No. 39.

Fairbrain, J., 1974, "A Reference Stress Approach to Creep Bending of Straight Tubes," *Journal of Mechanical Engineering Science*, Vol. 16, No. 3, pp. 125-138.

Ferber, M. K., Jenkins, M. G., and Tennery, V. J., 1990, "Comparison of Tension, Compression, and Flexure Creep for Alumina and Silicon Nitride Ceramics," *Ceramic Engineering Science Proceedings*, Vol. 11, No., 7, pp. 1028-1045.

Ferber, M., and Jenkins, M., 1992, "Evaluation of the Strength and Creep-Fatigue Behavior of Hot Isostatically Pressed Silicon Nitride," *Journal of the American Ceramic Society*, Vol 75, pp. 2453--2462.

Ferber, M., Jenkins, M., Nolan, T., and Yeckley, R., 1994, "Comparison of the Creep and Creep Rupture performance of Two HIPed Silicon Nitride Ceramics," *Journal of the American Ceramic Society*, Vol. 77, pp. 657-665.

Fields, B A., and Wiederhorn, S. M., 1996, "Creep Cavitation in a Siliconized Silicon Carbide Tested in Tension and Flexure," *Jaurnal of the American Ceramic Society*, Vol. 79, No. 4, pp. 977-986.

Hayhurst, D., Dimmer, P., and Chernuka, M., 1975, "Estimates of the Creep Rupture of Lifetime of Structures Using the Finite Element Method," *Journal of Mechanical Physics of Solids*, Vol. 23, pp. 335-355.

Hockey, B. J., and Wiederhorn, S. M., 1992, "Effect of Microstructure on the Creep of Siliconized Silicon Carbide," Journal of the American Ceramic Society, Vol. 75, No. 7, pp. 1822-1830.

Jadaan, O. M., Shelleman, D. L., Conway, J. C. Jr., Mecholsky, J. J., and Tressler, R. E., 1991, "Prediction of the Strength of Ceramic Tubular Components: Part I-Analysis," *Journal of Testing and Evaluation*, pp. 181-191.

Jadaan, O. M., and Tressler, R. E., 1993, "Methodology to Predict Delayed Failure Due to Slow Crack Growth in Ceramic Tubular Components Using Data from Simple Specimens," *Journal of Engineering Materials and Technology*, Vol. 115, pp. 204-210.

Jadaan, O.M., Powers, L. M., Nemeth, N. N., and Janosik, A., 1995, "Design of High Temperature Ceramic Components Against Fast Fracture and Time-Dependent Failure Using CARES/LIFE," *Ceramic Transactions, Design for Manufacturability of Ceramic Components*, Vol. 50, pp. 121-133.

Jones, D., 1986, "Phenomenological Analysis of Time-Temperature Mechanical Behavior of Ceramic Materials," *Proceedings 10th Annual Conference on Composites and Advanced Ceramic Materials*, Cocoa Beach, Fl.

Kachanov, L., 1960, *The Theory of Creep*, English Translation, Kennedy, A., ed., British Library, Wetnerley.

Khandelwal, P. K., Provenzano, N. J., and Schneider, W. E., 1995, Life Prediction Methodology for Ceramic Components of Advanced Vehicular Heat Engines-Final Report, Ceramic Technology Project, Oak Ridge National Lab.

Kraus, H., 1980, *Creep Analysis*, John Wiley and Sons Inc, New York.

Kromp, K., Haug, T., Pabst, R. F., and Gerold, V., 1987, "C* for Ceramic Materials? Creep Crack Growth at Extremely Low Loading Rates at High Temperatures Using Two-Phase Ceramic Materials," in Creep and Fracture of Engineering Materials and Structures, Wilshire, B., and Evans, R. W., Edts., pp. 1021-1032.

Lange, F., 1976, "Interrelations Between Creep and Slow Crack Growth for Tensile Loading Conditions," *International Journal of Fracture*, Vol. 12, pp. 739-744.

Larson, F., and Miller, J., 1952, "A Time-Temperature Relationship for Rupture and Creep Stresses," *Transactions ASME*, Vol. 74, pp. 765-771.

Lewis, G., and Ostvoll, A., 1992, "Constitutive Equations for the Creep of a Silicon Carbide Whisker-Reinforced Polycrystalline Alumina Composite Material," *Journal of the American Ceramic Society*, Vol. 75, No. 12, pp. 3481-3484.

Luecke, W., Wiederhorn S., Hockey, B., and Long, G., 1993, "Cavity Evolution During Tensile Creep of Si_3N_4," *Materials Research Society Symposium Proceedings*, Vol. 287, pp.467-472.

Manson, S., and Ensign, C., 1971, "A Specialized Model for Analysis of Creep-Rupture Data by the Minimum Commitment Method, Station-Function Approach," NASA TM-X-52999.

Maruyama, K., and Oikawa, H., 1987, "On Physical Bases of the Modified Projection Concept," *Proceedings of the 3rd International Conference on Creep and Fracture of Engineering Materials and Structures*, Wilshire and Evans, eds.

Menon, M., Fang, H., Wu, Jenkins, M., Ferber, M., More, K., Hubbard, C., and Nolan, T., 1994a, "Creep and Stress Rupture Behavior of an Advanced Silicon Nitride: Part I, Experimental Observations," *Journal of the American Ceramic Society*, Vol. 77, pp. 1217-1227.

Menon, M., Fang, H., Wu, D., Jenkins, M., and Ferber, M., 1994b, "Creep and Stress Rupture Behavior of an Advanced Silicon Nitride: Part III, Stress Rupture and Monkman-Grant Relationship," *Journal of the American Ceramic Society*, Vol. 77, pp. 1235-1241.

Monkman, F., and Grant, N., 1956, "An Empirical relationship Between Rupture Life and Minimum Creep Rate in Creep-Rupture Test," *Proceedings of the American Society for Testing and Materials*, Vol. 56, 593-620.

Morrell, R., and Ashbee, K. G., 1973, "High Temperature Creep of Lithium Zinc Silicate Glass-Ceramics, Part 1, General Behavior and Creep Mechanisms," *Journal of Materials Science*, Vol. 8, pp. 1253-1270.

Norton, F., 1929, *The Creep of Steel at High Temperatures*, McGraw-Hill.

Odqvist, F. K. G., 1974, *Mathematical Theory of Creep and Creep Rupture*, Oxford University Press.

Ohji, T., and Yamauchi, Y, 1993, "Tensile Creep and Creep Rupture Behavior of Monolithic and SiC-Whisker-Reinforced Silicon Nitride Ceramics," *Journal of the American Ceramic Society*, Vol. 76, pp. 3105-3112.

Orr, R., Sherby, O., and Dorn, J., 1954, "Correlations of Rupture Data for Metals at Elevated Temperatures," *Transactions American Society for Metals*, Vol. 46, p. 113.

Othman, A., and Hayhurst, D., 1990, "Multiaxial Creep Rupture of a Model Structure Using A Two Parameter Material Model," *International Journal of Mechanical Science*, Vol. 32, pp. 35-48.

Powers, L. M., Jadaan, O. M., Gyekenyesi, J. P., 1997, " Creep Life of Ceramic Components Using a Finite Element Based Integrated Design Program (CARES/*Creep*)," ASME paper 96-GT-369.

Quinn, G. D., 1986, "Static Fatigue Resistance of Hot Pressed Silicon Nitride," *Fracture Mechanics of Ceramics Vol. 8*, Bradt et al. eds., Plenum Press, pp. 319-332.

Quinn, G. D., 1990, "Fracture Mechanism Maps for Advanced Structural Ceramics, Part 1, Methodology and Hot Pressed Silicon Nitride Results," *Journal of Materials Science*, Vol. 25, pp. 4361-4376.

Sankar, J., Krishnaraj, S., Vaidyanathan, and Kelkar, A., 1994, "Elevated Temperature Behavior of Sintered Silicon Nitride Under Pure Tension, Creep, and Fatigue," *Life Prediction Data and Methodologies for Ceramic Materials, ASTM STP 1201*, Brinkman, C. R. and Duffy, S. F., eds., American Society for Testing and Materials, Philadelphia, pp. 19-35.

Shelleman, D. L., Jadaan, O. M., Conway, J. C. Jr., and Mecholsky, J. J., 1991, "Prediction of the Strength of Ceramic Tubular Components: Part I-Analysis," *Journal of Testing and Evaluation*, pp. 192-200.

Timoshenko, S., 1968, *Strength of Materials, Part II, Advanced Theory and Problems*, Princeton, van Nostrand.

White, C., and Hazime, R., 1995, "Internal Variable Modeling of the Creep of Monolithic Ceramics," *Proceedings of the 11th Biennial Conference on Reliability, Stress Analysis, and Failure Prevention*, Editor, Jadaan, O., ASME, Philadelphia, PA.

Wiederhorn, S. M., Roberts, D. E., Chuang, T.-J., and Chuck, L., 1988, "Damage Enhanced Creep in a Siliconized Silicon Carbide:

Phenomenology," *Journal of American Ceramic Society*, Vol. 71, pp. 602-608.

Wiederhorn, S., Quinn, G., and Krause, R., 1994, "Fracture Mechanism Maps: Their Applicability to Silicon Nitride," *Life Prediction Methodologies and Data for Ceramic Materials*, ASTM STP-1201, Brinkman, C. R., and Duffy, S. F., eds., American Society for Testing and Materials, Philadelphia, pp. 36-61.

Wilkinson, D. S., Caceres, C. H., and Robertson, A. G., 1991, "Damage and Fracture Mechanisms During High-Temperature Creep in Hot-Pressed Alumina," *Journal of the American Ceramic Society*, Vol. 74, No. 5, pp. 922-933.